JOURNAL OF THE MECHANICAL BEHAVIOR OF BIOMEDICAL MATERIALS 28 (2013) 383–392

Available online at www.sciencedirect.com

ScienceDirect

www.elsevier.com/locate/jmbbm

Research Paper

Indentation of poroviscoelastic vocal fold tissue using an atomic force microscope ☆

Hossein K. Heris[a], *Amir K. Miri*[a,*], *Umakanta Tripathy*[b,c], *Francois Barthelat*[a], *Luc Mongeau*[a]

[a]*Biomechanics Laboratory, Department of Mechanical Engineering, McGill University, 817 Rue Sherbrooke Ouest, Montreal, Que., Canada H3A 0C3*
[b]*Department of Physics, McGill University, 3600 Rue University, Montreal, Que., Canada H3A 2T8*
[c]*Department of Chemistry, McGill University, 3600 Rue University, Montreal, Que., Canada H3A 2T8*

ARTICLE INFO

Article history:
Received 26 September 2012
Received in revised form
18 May 2013
Accepted 27 May 2013
Available online 14 June 2013

Keywords:
Indentation
Anisotropy
Permeability
Atomic force microscopy
Nonlinear optics
Vocal folds

ABSTRACT

The elastic properties of the vocal folds (VFs) vary as a function of depth relative to the epithelial surface. The poroelastic anisotropic properties of porcine VFs, at various depths, were measured using atomic force microscopy (AFM)-based indentation. The minimum tip diameter to effectively capture the local properties was found to be 25 μm, based on nonlinear laser scanning microscopy data and image analysis. The effects of AFM tip dimensions and AFM cantilever stiffness were systematically investigated. The indentation tests were performed along the sagittal and coronal planes for an evaluation of the VF anisotropy. Hertzian contact theory was used along with the governing equations of linear poroelasticity to calculate the diffusivity coefficient of the tissue from AFM indentation creep testing. The permeability coefficient of the porcine VF was found to be $1.80 \pm 0.32 \times 10^{-15}$ $m^4/N\,s$.

1. Introduction

Mechanical elastic properties are important to ensure the functionality of remodeled engineered tissue constructs. The design of biomimetic injectable biomaterials requires information about the specific elastic properties of the host tissue (Heris et al., 2012). Changes in elastic properties associated with pathology can be best captured if characterized at the microscale (Athanasiou et al., 2000; Loparic et al., 2010). Indentation at different length scales has been frequently used for the mechanical characterization of materials. Indentation methods are well suited to soft biological material and can be used to map the mechanical properties of inhomogeneous biological tissues. Indentation at the microscale requires only a very small sample volume, on the order of 100 μL, which is especially helpful in studies using small animal models, such as rats.

The indentation of very soft tissue with elastic moduli on the order of kiloPascals requires high resolution measurements in terms of force and displacement. The indentation depth for a thin layer of such tissue should not exceed 10% of the sample thickness (Butt et al., 2005). Beyond this region,

☆This paper was presented at the Fourth International Conference on the Mechanics of Biomaterials and Tissues (ICMOBT4).

*Corresponding author. Tel.: +1 514 661 1363; fax: +1 514 398 7365.
E-mail addresses: amir.miriramsheh@mail.mcgill.ca, akmiri@gmail.com (A.K. Miri).

1751-6161/$ - see front matter © 2013 Elsevier Ltd. All rights reserved.
http://dx.doi.org/10.1016/j.jmbbm.2013.05.026

the tissue material may exceed linear elasticity because soft tissues undergo large deformations, and indentation results may be affected by substrate properties. Indentation forces depend on the indentation depth, probe size and elastic modulus of the sample. An atomic force microscope (AFM) with colloidal probes can overcome the resolution limitations of conventional indenters (Stolz et al., 2004). It can be used to image the topographical features of a small tissue sample and measure local elastic properties through indentation at different length scales depending on the probe size.

The vocal fold (VF) is inhomogeneous, anisotropic, and fluid-saturated porous. The VFs are located at the top of the trachea and under the epiglottis (Fig. 1a). They are stretched horizontally across the larynx along the anterior–posterior direction (Fig. 1b). To evaluate the inhomogeneity of the VFs, the tissue sample should be sliced to probe at different depths. This technique was recently applied to ex-vivo brain tissue to assess the elasticity of gray and white brain matter (Kaster et al., 2011). To investigate the mechanical anisotropy, indentation was performed for bone samples sectioned in planes along different orientations relative to the material axes, used for hard tissues such as bone (Fan et al., 2002; Swadener et al., 2001). In another approach, structural data was used to estimate the anisotropic properties of osteon lamellae through the implicit calculation of material constants fitted to measured indentation data (Reisinger et al., 2011). These techniques have not yet been adapted for the characterization of soft tissues, including the VFs. Conventional testing methods along with a transversely isotropic model were used to determine the anisotropic mechanical properties of porcine VFs (Miri et al., 2012b). Pipette aspiration method is another technique for characterization of the local, anisotropic properties of the VFs (Weiß et al., 2012).

Poroelastic models treat the tissue as a porous structure with deformable solid and penetrating fluid phases (Galli and Oyen, 2009). Upon mechanical loading, the solid phase undergoes normal and shear stresses while the fluid phase experiences hydrodynamic pressure. In a numerical study, a continuous poroelastic linear model of VF was developed to simulate the liquid flow in the tissue and study the fluid dynamics during VF oscillations (Tao et al., 2009). No empirical data was presented on the permeability of VF tissue. The

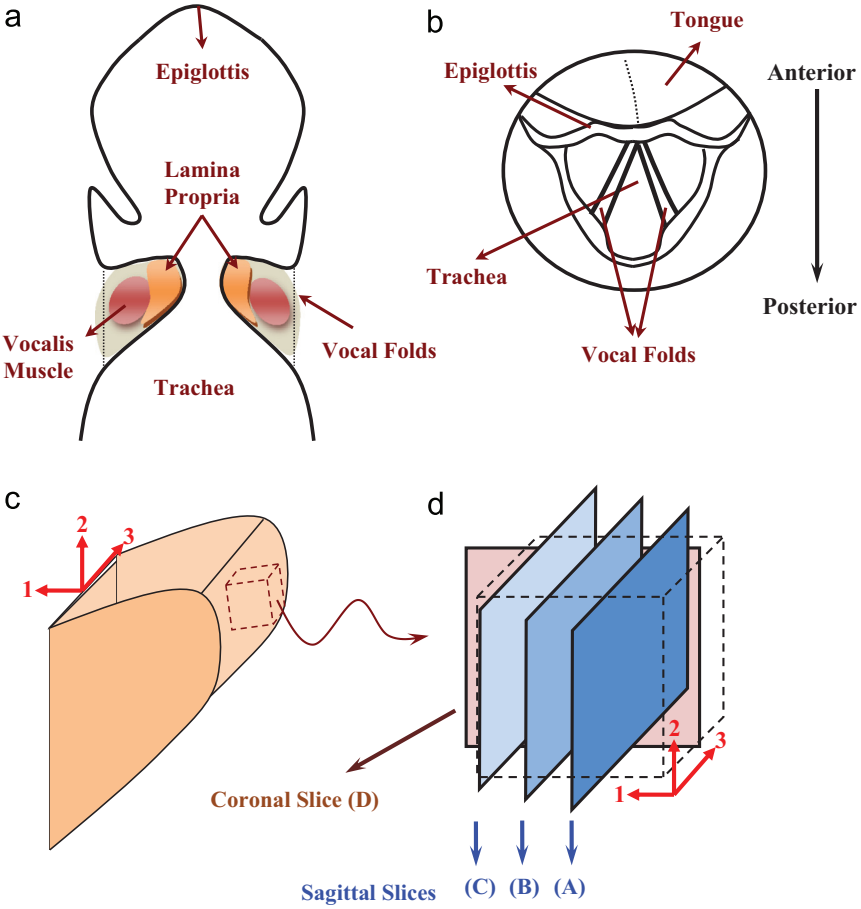

Fig. 1 – (a) Coronal view of larynx. (b) Transverse view of Larynx. (c) Sketch of one vocal fold and material coordinate system. A small cubical portion of the tissue is shown by the dashed lines. The location was around one third of the span near the thyroid cartilage, where the impact stress is believed to be the greatest. (d) Cubic tissue sample was then sectioned in three sagittal slices shown in blue (A, B, C), and one coronal slice (D) shown in pink. A is the superficial layer, closer to the surface of the vocal folds. B is the intermediate layer and C is the deep layer of the vocal folds. Direction 3 is the anterior–posterior direction. Direction 2 is the inferior-superior direction and direction 1 is the medial-lateral direction. The sagittal planes are denoted as 1-planes (perpendicular to direction 1) and coronal planes as 3-planes (perpendicular to direction 3).
(For interpretation of the references to color in this figure legend, the reader is referred to the web version of this article.)

same study emphasized the importance of poroelastic models in studying pathological conditions such as VF dehydration, nodules and polyps.

A first attempt at measuring VF elastic properties at different depths was recently made using conventional indentation testing (Chhetri et al., 2011). The body and cover layers in human VFs were harvested using scissor dissection, and the tests were done in air. Errors originating from surface roughness were compensated for by the use of a large indenter, at the cost of lower spatial resolution. The goal of the present study is to characterize the poroelastic properties of the porcine VF using AFM-based indentation testing. Porcine VFs have a heterogeneous structure similar to that of humans VFs (Hahn et al., 2006a, 2006b). The collagen fibers in the VF are dominantly aligned along the anterior-posterior direction, which is believed to cause anisotropic behavior. Uniaxial tests yield VF elastic properties (Miri et al., 2012a) but do not provide anisotropic information. Biaxial tests are challenging because of the limited VF width and a tendency for delamination upon transverse traction loads. Indentation tests were used in the present work to capture heterogeneoity, anisotropy and poroelastic properties of porcine VFs. The procedures followed can eventually be used to characterize human or animal VFs, tissue-engineering constructs, or any other soft tissue.

2. Materials and methods

2.1. Tissue preparation

Healthy porcine larynges were obtained immediately postmortem and immersed in a normal saline solution. Dissection was performed using established protocols (Miri et al., 2012a). Sharp blades were used to excise an area of around 2 mm × 2 mm from the central region of the VF lamina propria within the sagittal plane. The sample thickness was between 1 and 2 mm within the VF (Hahn et al., 2006a, 2006b). The tissue was flash frozen in an OCT (Optimal Cutting Temperature Compound, Sakura Finetek, Dublin, OH) medium with no labeling or dehydration. The dissected tissue cube was cut into two pieces by a coronal cut to obtain three sagittal (1-plane) slices from one half and one coronal (3-plane) slice from the other half. The tissues were sectioned using a cryostat (Leica CM-3505-S). To obtain the three 1-plane slices, layers with an equal thickness of 50 μm were removed at 100 μm depth intervals, starting from the epithelium (Fig. 1d). One 50 μm 3-plane slice was cut from the other half (Fig. 1d). The samples were placed over a very thin layer of nail polish on a microscopy glass slide. The nail polish was used to glue the tissue to the glass substrate. The first three 1-plane slices were subjected to the indentation and creep tests and one 3-plane slice was subjected to the indentation test. To probe the inhomogeneity of the VF tissue along the anterior–posterior direction, the entire lamina propria, around 15–18 mm in load-free length, was dissected.

2.2. Nonlinear laser scanning microscopy

Nonlinear laser scanning microscopy (NLSM) was used for simultaneous imaging of the collagen and elastin distributions within the samples. A custom-built, dual-mode NLSM system was used (Miri et al., 2012c). The procedure allowed second harmonic generation (SHG) and two-photon fluorescence (TPF) microscopy to be performed simultaneously with high spatial resolution. The excitation wavelength was 1050 nm, and the scattered signals were detected with SHG detection channel (Chroma, HQ525/50m-2p) and TPF detection channel (Chroma, HQ600/50-2p), both in the forward direction. The SHG and TPF images were recorded in TIF format and then merged with the open-source *ImageJ* software (NIH; Bethesda, MD). The SHG channel displays the collagen microstructure, and the TPF channel displays the elastin network (Miri et al., 2012c).

2.3. Indentation and creep tests using AFM

Indentation tests were performed using a Veeco multimode AFM with a NanoScope V controller. Two different types of colloidal probes (Novascan technologies Inc., Ames, IA, USA) were tested: (1) soft cantilever with a nominal stiffness of 0.06 N/m and a probe diameter of 4.5 μm, and (2) stiffer cantilevers with nominal stiffnesses of 1.75 N/m and 7.5 N/m, and a probe diameter of 25 μm. The deflection sensitivity of the piezo module was established by probing the surface of the glass substrates. A thermal tuning method was used to calibrate the stiffness of the cantilevers. An area of 100 μm × 100 μm was indented around the center of each sample. A liquid cell for the AFM cantilever was used to perform the experiments under phosphate buffer solution. Indentation and indentation creep tests were performed at room temperature on the samples, prepared as described above. Three samples ($n=3$, total of 12 slices) were indented using a ramp function, with constant velocity loading and unloading. Unloading was started immediately after the load reached a maximum. To avoid permanent deformation, the unloading data was used as a basis for the determination of the indentation modulus. The model proposed by Oliver and Pharr (1992) was used to infer the elastic properties from the measured data.

Three other samples ($n=3$, total of 9 slices) were indented using a ramp-hold function, as in a creep test. A quasi-static loading was applied with a constant velocity of 4 μm/s until the maximum force was measured. Then the force was held constant before unloading was initiated. For the creep tests, scripts were added and run in the ramp force window of the Nanoscope software (version 7.30), which controls the AFM hardware. A relative set point of 5 to 10 V, associated with a force range from 50 to 200 nN, was used. The set point associated with the cantilever deflection was kept constant over a period of 100 seconds. In this mode of operation, the deflection of the cantilever was kept constant through feedback control and adjustments at the base of the cantilever. The translational displacement of the base of the cantilever and the force (constant value) were recorded as a function of time. The creep data was used to extract the diffusivity coefficient of each slice.

All sectioned slices were kept frozen before AFM tests to minimize the errors originating from the enzymatic degradation of tissue in room temperature. For each tissue slice, a time period of 30–45 min was needed to prepare the setup and perform the indentations.

2.4. Calibration of the AFM force and displacement data

Force signals were filtered to remove high-frequency noise using Matlab[c]. The location of the contact point was determined from the sudden change in the force deflection curve. Identification of the exact point of contact is a challenge of using AFM for soft material characterization, especially in the presence of adhesion forces (Rahmat and Hubert, 2010). These forces can induce non-contact interaction stresses between the contacting bodies. For most samples, small adhesion forces were observed. To account for this, the location of the initial repulsion force on the displacement axis (cantilever translational axis) was considered as the contact point (Z_0). Force at the point of contact (F_0) should be zero; thus, the force data was scaled to compensate for the offset and to enforce the zero value. The indentation depth (h) was calibrated according to the equation (Lin et al., 2007)

$$h = (z - z_0) - (d - d_0), \tag{1}$$

where z is the displacement of the cantilever base, d is the deflection of the cantilever, and d_0 is the deflection of the cantilever at the point of contact. The deflection of the cantilever was calculated from measured force values using

$$d - d_0 = F/k, \tag{2}$$

where F is the force and k is the stiffness of the cantilever.

2.5. Determination of the indentation modulus

The unloading curves were analyzed to determine the elastic moduli of the tissue. A power-law relation was used to perform a regression of the part of the unloading curve near the maximum depth. The indented load, F, was found to obey the relation (Oliver and Pharr, 2004)

$$F = b(h - h_f)^m, \tag{3}$$

where m and b are constants obtained from curve fitting, h is the vertical displacement of the indenter, and h_f is the final unloading depth. For spherical indentors, $m=1.5$ is typically used (Oliver and Pharr, 2004). The indentation modulus, E^*, can be obtained from

$$E^* = \frac{\sqrt{\pi}}{2}(1-\upsilon^2)\frac{S}{\sqrt{A}}, \tag{4}$$

where υ is Poisson's ratio, S is the contact stiffness, and A is the effective contact area. The contact stiffness (S) of the tissue was estimated from the slope of the unloading indentation curve at the inception. To minimize the error associated with the nose effect often observed in the inception part of the unloading curve for viscoelastic materials (Ebenstein and Pruitt, 2006), the upper 25% of the unloading curve was used to calculate the contact stiffness from a linear regression. When the loading ends, the tissue continues to creep and water drainage continues during unloading. The greater rate of creep from loading compared to the tissue recovery rate from unloading causes the nose effect. For a spherical indenter with radius R indenting a semi-infinite half-space, the contact area is (Oliver and Pharr, 2004)

$$A = \pi(2Rh_C + h_C^2), \tag{5}$$

where h_c is the contact depth, determined from

$$h_C = h_{max} - \gamma F_{max}/S, \tag{6}$$

and h_{max} is the maximum indentation depth, F_{max} is the maximal indenter load at h_{max}, and γ is a constant that depends on the geometry of the indenter. A value of 0.75 is normally used for spherical probes (Oliver and Pharr, 2004).

The elastic moduli (E_1^*, E_3^*) obtained from indentation in 1- and 3-planes were used to define a new anisotropy index, i.e., $AI = E_1^*/E_3^*$. This ratio estimates the anisotropic mechanical properties of transversely isotropic VF tissue.

2.6. Poroelastic modeling

The avascular nature of the lamina propria requires relatively free movement of interstitial fluid among cellular components and extracellular matrix proteins. This suggests a porous distribution of the underlying structure in the VF tissue, as observed by NLSM and AFM (Miri et al., 2013). Classical poroelastic theory has been used to simulate biological soft tissues, such as the blood vessel epithelial layer (Miri and Mitri, 2011). A similar framework was used here based on the classical 1-D *consolidation* problem. A schematic of the uniaxial consolidation test is shown in Fig. 2(a). The saturated poroelastic material of known thickness, L, is surrounded by two impermeable walls and two permeable boundaries along the direction of loading. Hence, the material model is fully drained, with L chosen such that pressure vanishes on both sides.

For a material model subjected to uniaxial strain, ε_x (Fig. 2), the constitutive equation for the non-vanishing stress component is (Galli and Oyen, 2009)

$$\sigma_x = \frac{2G(1-\upsilon_u)}{1-2\upsilon_u}\varepsilon_x - \alpha p, \tag{7}$$

In the above equation, G and ν_u are the shear modulus and Poisson's ratio of the drained material, p is the pore pressure, and α is the variation of the fluid volume as a result of volumetric changes within the range of $0 \le \alpha \le 1$. The shear

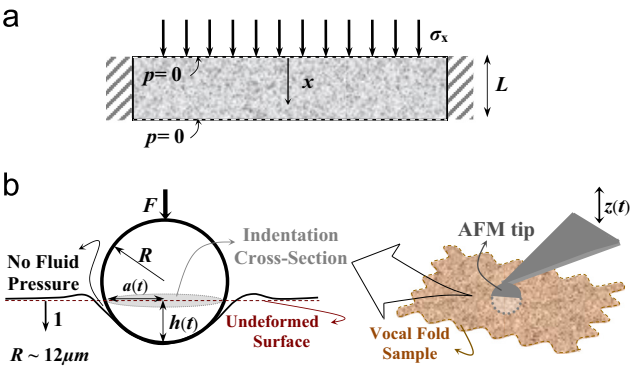

Fig. 2 – (a) One-dimensional consolidation test. The parameter L denotes the sample thickness, x is the local coordinate. (b) Indentation of one tissue sample using AFM and the deformation field around a spherical tip. z denotes the movement of the cantilever in vertical direction, F the contact force on the tip, R the tip radius, and h the indentation depth.

modulus, G, represents the resistance of the solid structure under quasi-static, shear loading. The tissue time-dependent properties are governed by fluid–solid interactions within poroelasticity theory; however, standard viscoelastic models include those effects in a single complex shear modulus. The fluid pressure was obtained from (Galli and Oyen, 2009)

$$p = \frac{2G(\upsilon-\upsilon_\circ)}{\alpha^2(1-2\upsilon)(1-2\upsilon_\circ)}(\zeta-\alpha\varepsilon_x), \tag{8}$$

where ν is the undrained Poisson's ratio and ζ is the variation of fluid volume subjected to the local continuity equation,

$$\zeta_{,t} + q_{x,x} = 0. \tag{9}$$

The subscript comma denotes partial differentiation with respect to time or position. The specific discharge vector, q_x, which is the rate of fluid volume crossing a unit area, is related to the permeability coefficient, κ, through Darcy's law, expressed as

$$q_x = -\kappa p_{,x}. \tag{10}$$

From Eqs. (7)–(10), the governing diffusion equation for the pore pressure is then obtained as (Galli and Oyen, 2009)

$$p_{,t} - Dp_{,xx} + \frac{\nu-\nu_\circ}{\alpha(1-2\nu_\circ)(1-\nu)}\sigma_{x,t} = 0, \tag{11}$$

where the diffusivity coefficient, D, is obtained from

$$D = \frac{2\kappa G(1-\nu_\circ)(\nu-\nu_\circ)}{\alpha^2(1-2\nu_\circ)^2(1-\nu)}, \tag{12}$$

Eqs. (7)–(12) govern the solutions to consolidation poroelastic problems. Based on previous studies (Galli and Oyen, 2009), consolidation poroelastic equations were extended to the classic indentation problem with a spherical indenter (Johnson, 1987), in which case the characteristic length is assumed to be the one-dimensional projection of the contact area. Using a Hertzian model, it may be rewritten as $L = 2 \times R\cos^{-1}((R-h_\infty)/R)$ where R and h_∞ are the tip radius and the steady-state indentation depth, respectively (Nia et al., 2011). The samples were subjected to a series of ramp-hold tests. Following a ramp loading with a rate of $\sigma_{x,t} = \bar{\sigma}$ from $t = 0$ to $t = t_R$, the sample was maintained at a load of $\sigma_x(t = t_R)$ for a time period sufficiently long to reach steady-state. The pressure field, $p(x,t)$, may be obtained from Eqs. (8)–(10) and then used to express $u_x(x,t)$ using the well-known relation $\varepsilon_x = u_{x,x}$ (Galli and Oyen, 2009). For the thickness function, $u_x(0,t) \equiv h(t)$, one may estimate the corresponding time constant using a first order approximation,

$$h(t) = h_\infty + (h_\circ - h_\infty)\exp(-t/\tau), \tag{13}$$

where $h_\circ$ and h_∞ represent the initial and final thickness or indentation depths, respectively. Eq. (13) was used to obtain a regression of the displacement–time histories. The diffusivity coefficient was calculated from the master curves provided by Galli and Oyen (2009) for $\alpha = 1$, and $\nu = 0.5$, as

$$D = 0.08\frac{L^2}{\tau}. \tag{14}$$

Therefore, two other poroelasticity constants (κ, $\nu_\circ$) can be obtained from Eq. (12). In addition, the drained Poisson's ratio may be estimated by assuming a step-loading from Hertz's formula (Galli and Oyen, 2009)

$$\frac{h_\infty}{h_\circ} = \left(\frac{1-\nu_\circ}{1-\nu}\right)^{2/3}. \tag{15}$$

3. Results

3.1. *Identification of indenter size from structural data*

There is a practical lower limit to the indentation depth and indenter size for hierarchical materials. An excessively small indentation area may yield the mechanical properties of individual collagen bundles, elastin fibers, other macromolecules, or a mixture of these constituents rather than the tissue's overall bulk mechanical properties. Microstrucural data from the NLSM were used to determine the smallest possible probe size. Images over an area of 100 μm × 100 μm were used, which is sufficiently large to ensure the homogenized properties. The strength and the elasticity of soft tissues are mainly governed by the concentration of collagen and elastin fibers. Fig. 3(a) shows an SHG image of the VF collagen fibers, which are oriented mainly along the 1-plane. Fig. 3(b) shows an image of the elastin fibers in the tissue, as captured by the TPF channel. The elastin network has an isotropic distribution. The relative distribution of elastin and collagen fibers is shown in a combined image in Fig. 3(c).

To identify the minimum indentation area covering a representative distribution of bulk local properties, the color image shown in Fig. 3(c) was further analyzed on a gray scale. Fig. 4(a) shows the normalized distribution of light intensity in the gray scale image. The aim was to obtain the minimum area for which

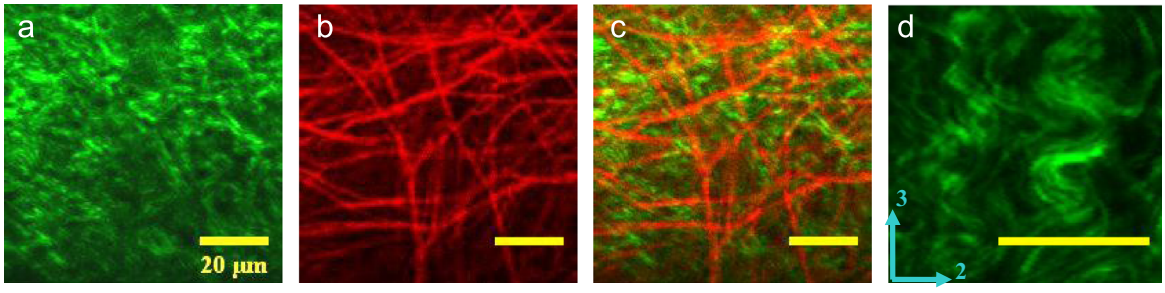

Fig. 3 – Nonlinear Laser Microscopy of the porcine lamina propria in sagittal plane (a) Second harmonic generation image of LP tissue revealing collagen. (b) Two-photon fluorescence microscopy of the LP tissue revealing elastin. (c) The superposition of images (a) and (b). (d) Magnified view of LP tissue showing anisotropic distribution of collagen fibrils in sagittal plane. The collagen fibers are mainly oriented in the anterior-posterior direction. The scale bar is 20 μm.

the distribution of gray pixels (fibers) remains a continuous Gaussian distribution similar to the original image. Each segment was then divided into smaller areas. The light intensity falls within one single Gaussian distribution for subsets having an area larger than the critical value, which in this case was 12.5 μm × 12.5 μm; that is, the distribution of fibers found within this subset area was representative of larger areas. For subsets with an area smaller than the critical value, the distribution density is subdivided into several distributions. Assuming an indentation depth of around 2 μm, an indenter with a diameter of 25 μm yields a contact area of around 12.5 μm × 12.5 μm. The effect of probe size variation was experimentally assessed using two probe sizes, with diameters of 25 and 4.5 μm, as shown in Fig. 5. The indentations were performed at different random points over a tissue area of 100 μm × 100 μm. The indentation curves for the larger probe are more uniform, resulting in an elastic modulus with a lower standard deviation. Indentation tests from the smaller probe resulted in discretized curves, indicating that individual macromolecules or combinations of fibers were indented instead of a representative network of constituents. This observation supports the selected minimum indenter size. The two curves show very different viscous losses. When the indenter size was small, fluid did not percolate through the porous structure and the viscoelasticity of the extracellular matrix mostly contributed to the viscous losses. The adhesion forces observed in the unloading curves were greater for the larger probe than for the smaller probe.

3.2. *Inhomogeneous and anisotropic elastic properties*

Fig. 6 shows the results of the indentation modulus for four different slices of the VF samples. For each VF tissue slice, two different areas in the center of each section were selected. Within each area, nine indentation tests were performed at different random points. Then the mean value was calculated for each porcine VF. The average of all mean values and the corresponding standard deviations were obtained. The indentation elastic moduli in the 1-planes (Fig. 1c) increase with depth from the superficial layer to the deep layer, which indicates that the mechanical properties are inhomogeneous across different layers. The indentation elastic modulus in the 3-plane was almost half the average value seen in 1-planes. Such anisotropic properties were expected from the NLSM images (Fig. 3d; Miri et al., 2013).

Fig. 7 shows the elastic properties along the second 1-plane for slice B. Three areas with equal distances were selected to cover the distance between the VF and the thyroid cartilage. The indentation elastic modulus increases from the central to the anterior part of the tissue, indicating a smooth

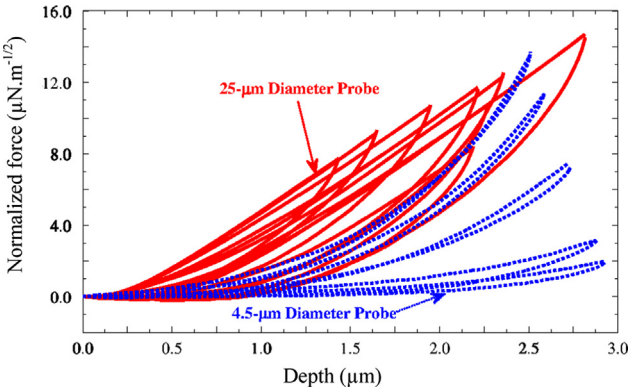

Fig. 5 – Indentation force vs. depth for probes of different sizes. The indentation force was divided by the square root of the diameter (force/[probe diameter]$^{1/2}$). A probe with a diameter of 25 μm yields more repeatable results (shown in red) with less variation compared to a probe with a smaller diameter (4.5 μm). Small adhesion force was observed in the unloading curve related to large diameter probe. (For interpretation of the references to color in this figure legend, the reader is referred to the web version of this article.)

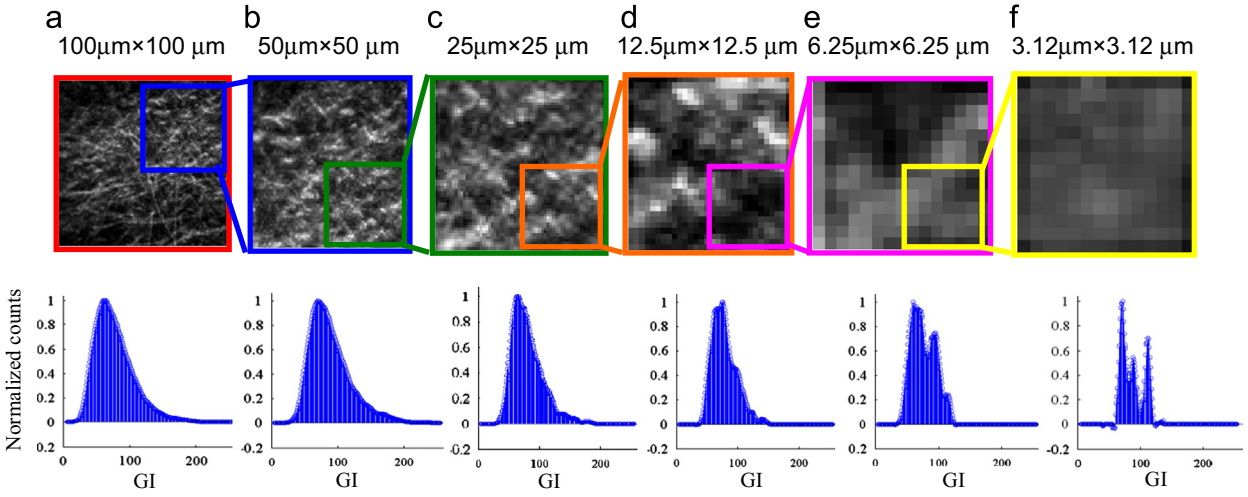

Fig. 4 – Image processing of the microscopic image. The intensity distribution is shown below each image. From left to right, each image is segmented into four subsets and one of the four segments is analyzed in the subsequent column. The distribution of intensity remains almost constant until column (d). The statistics change from column (e) suggesting that an area of 12.5 μm × 12.5 μm is the minimum value needed to obtain bulk properties of a local region of the tissue. The indentation of a smaller area may not reflect the continuum properties of the tissue. GI represents grayscale intensity.

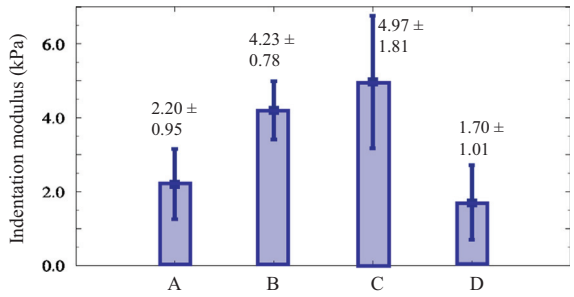

Fig. 6 – Indentation results on sagittal planes (A–C) and on the coronal plane (D). The stiffness of the tissue increases from the superficial (A) layer to the deep layers (B and C). The indention test on coronal section, D: the place of indentation corresponds to plane B, indicates a high level of anisotropy in vocal fold lamina propria tissue.

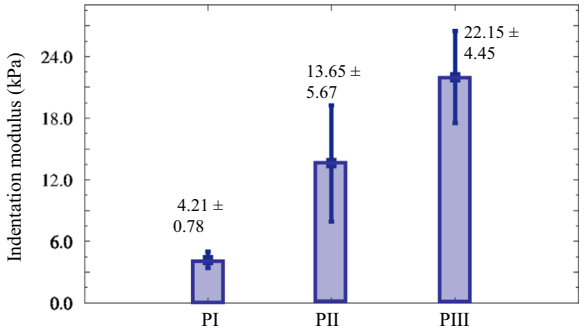

Fig. 7 – Indentation tests at three locations on the second sagittal slice (B) to scope the inhomogeneity of the tissue. PI is located at one-third the length of the vocal folds. PII is located at one-sixth of the length of the vocal folds. PIII is located near the thyroid cartilage.

transition from the tissue to the cartilage, and significant inhomogeneity along the anterior–posterior direction. The central part of the VF has the lowest stiffness where mucosal wave propagation occur, as observed in excised larynx studies (Bakhshaee et al., 2013). VF nodules and scarring normally appear within this region (Wallis et al., 2004).

3.3. *Permeability of porcine VF tissue*

A typical indentation creep test graph is shown in Fig. 8, along with an exponential curve fit. The starting point of creep test was affected by the antecedent quasi-static indentation and the exact starting point of creep could not be clearly identified. No constraint on the starting point of creep was applied in the curve-fitting algorithm to better fit the experimental data with the theoretical formulation. The fit was used to extract the time constant, τ, introduced in Eq. (13). The time constant was used to calculate the diffusivity coefficient using Eq. (14). Then, the permeability coefficient was calculated using Eq. (12). Table 1 shows the diffusivity coefficient and the permeability coefficient calculated from the indentation creep tests for 1-planes slices A, B and C. For each of the three slices, three different samples (nine slices in total) were subjected to creep tests. In Eq. (12), the shear

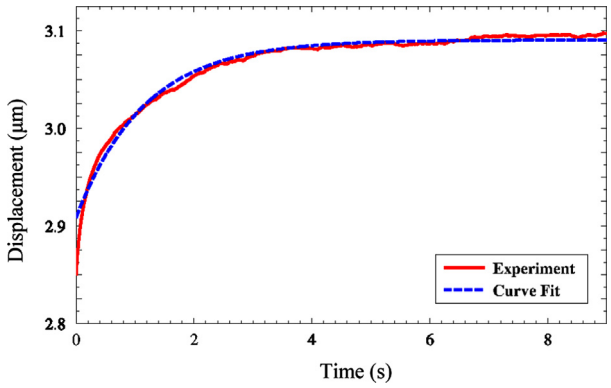

Fig. 8 – Typical indentation creep curve fitted with an exponential function of 3.09×10^{-6}–$1.83\times10^{-7}\times e^{-t/1.54}$, in which the time constant, τ, was found to be 1.54 s.

modulus value, G, was computed from the indentation result in each slice using the following equation:

$$G=\frac{E_1^*}{2(1+\nu)}, \tag{16}$$

where E_1^* is the elastic modulus measured from indentation tests in the 1-plane.

4. Discussion

4.1. *AFM-based indentation*

Indentation tests using AFM are subject to different types of error. The first is due to spring constant calculations using thermal noise methods (around 15% error). Another source of error is surface roughness, which may be compensated through the use of a greater indentation depth. One other type of error results from the nonlinearity of the AFM cantilever. Cantilevers with high spring constants lack force resolution, while those with low spring constants may not indent deep enough or stay linear at deeper indentations. The required spring constant for cantilevers used as micro-indenters probing locally homogenized properties of soft substrates can be approximated by combining the Hertz contact theory with the principles of AFM force measurement, and assuming AFM cantilever as simple harmonic oscillator ($F=Kd$), following equation

$$K\approx\frac{4E}{3(1-\upsilon^2)\delta_{max}}R^{1/2}h_{max}^{3/2}, \tag{17}$$

where K is the stiffness of the cantilever, E is the approximate Young's modulus, R is the radius of the indenter, h_{max} is the maximum required indentation depth, and δ_{max} is the maximum cantilever deflection that preserves linear sensitivity. Structural data can be used to calculate h_{max} and R. Most cantilevers remain linear up to a deflection of 100 nm. Those used in this study had an upper limit of 50–200 nm. Cantilever with nominal stiffness $K=1.75$ N/m was found to provide better results in terms of sensitivity (signal to noise ratio) for force measurement and rigidity for indention of the tissue.

Table 1 – Diffusivity coefficient (m^2/s) and permeability ($m^4/N\ s$) f the vocal fold lamina propria in different sagittal planes obtained from AFM creep test.

	Diffusivity coefficient (D) mean ± standard deviation	Permeability coefficient (κ) mean ± standard deviation
1st Layer (A)	$1.62 \times 10^{-11} \pm 7.92 \times 10^{-12}$	$2.30 \times 10^{-15} \pm 1.03 \times 10^{-15}$
2nd Layer (B)	$1.59 \times 10^{-11} \pm 1.01 \times 10^{-11}$	$2.00 \times 10^{-15} \pm 9.75 \times 10^{-16}$
3rd Layer (C)	$7.83 \times 10^{-11} \pm 3.33 \times 10^{-12}$	$1.11 \times 10^{-15} \pm 4.48 \times 10^{-16}$

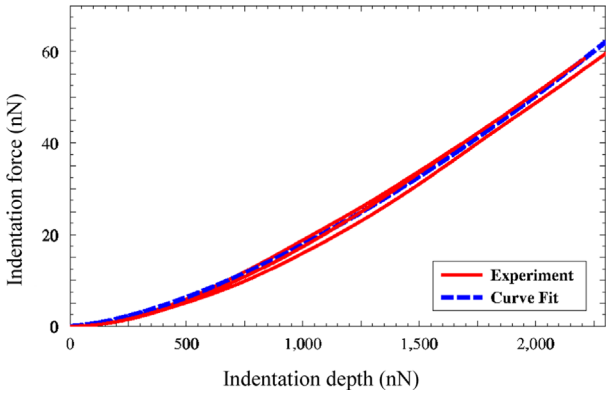

Fig. 9 – Hertzian curve fitting on three sample loading data. The indentation curves show Hertzian behavior.

Finally, it should be noted that inherent variations in the thickness of the VF in different animals led to relatively higher standard deviations for the elastic modulus measurement in slice C (Fig. 1d). In some cases, the slice C lies at the junction between the VF lamina propria and vocalis muscle. In other cases, it is entirely within the VF.

The use of a model with a closed form solution for an isotropic material is convenient for analysis. But, anisotropic materials experience asymmetric deformation, which may have introduced errors. There is no explicit solution to extract the elastic engineering constants along the principal axes of the material.

Each tissue sample with a thickness of 50 μm was indented to a depth of 3 ± 0.5 μm, or 6% of the thickness. This percentage is below the limit of 10 to 20%, where indentation curves start to become nonlinear because of the substrate effects. The indentation depth corresponds to 12% of the indenter diameter. The mean indentation strain ($\varepsilon \approx 0.2a/R$ (Lin et al., 2009)) was approximately 13% for our measurements. At indentation depths of 3 ± 0.5 μm, force vs. indentation curves obeyed the Hertz contact model and confirmed the applicability of linear elasticity (Fig. 9).

The volume fraction of collagen fibers in the porcine VF is equal to that of human VF based on histological analysis (Hahn et al., 2006b). Tensile tests on porcine and human VF ligaments (intermediate and deep layers) yielded similar results (Alipour et al., 2011; Kelleher et al., 2012). Indentation of the medial parts of human VFs has yielded a modulus of 4.4 ± 1.9 kPa, using an indenter with a 1-mm diameter. The results are similar to the indentation modulus of 4.2 ± 0.4 kPa obtained in our work using an AFM probe with a diameter of 25 μm. This similarity indicates that micrometer-scale characterization of VF tissue would yield bulk mechanical properties measured at the millimeter scale. It also supports the analysis used to define the minimum indenter size.

4.2. *Anisotropy and inhomogeneity of VF tissue*

The results confirm the existence of anisotropic mechanical stiffness, which was expected from structural data generated through NLSM and other histological techniques (Miri et al., 2013). The anisotropy index, AI = 2.47, indicates that VF tissue is highly anisotropic. In general, indentation tests underestimate the anisotropic mechanical properties relative to results from axial tests along the principal axes of the material. For instance, indentation of osteons in two perpendicular planes resulted in an anisotropy ratio of 1.3, whereas calculation of elastic constants in the principal axis resulted in a ratio of approximately 2 (Reisinger et al., 2011). The ratio is larger for porcine VFs because most of the collagen fibers are aligned along the anterior-posterior length (Miri et al., 2013 and Fig. 3), although it is less pronounced than in human VFs (Miri et al., 2012c).

A transversely isotropic material model, with the 3-plane as the plane of isotropy, has been commonly used for VFs (Titze and Talkin, 1979). It has five independent engineering constants (E_{11}, E_{33}, G_{13}, ν_{12}, and ν_{13}), which reduces to a set of three independent constants (E_{11}, E_{33}, and G_{13}) for incompressible materials (Itskov and Aksel, 2002). The elastic properties of a tissue are a function of the configuration and the elasticity of collagen, elastin, and glycosaminoglycans, the main constituents of VF tissue. The constant E_{33} is mostly determined by the collagen fibers because of their alignment along the 3-direction. Elastin and glycosaminoglycans are assumed to have an isotopic distribution. Indentation in the 3-plane may not be affected by collagen fibers because they mostly contribute to the tensile stiffness of the tissue. Compression loads of the tissue are sustained by glycosaminoglycans, assumed to be uniformly distributed in the tissue. Thus, one can assume that indentation along 3-direction can be considered as an indentation test on an isotropic material with $E_{iso} = E_{11}$, which yields $E_{11} = E_3^* \approx 1.7 \pm 1.1$ kPa as the transverse modulus of VF. The calculated value is in the range of the transverse modulus for human VF ligaments (intermediate and deep layers of the VF) reported in the literature ($E_{11} = 2.5 \pm 1$ kPa) (Kelleher et al., 2012).

Indentation along 1-direction could not be related to the longitudinal elastic moduli without further analysis. A general solution for the indentation of anisotropic half spaces has been presented in the literature (Swadener and Pharr, 2001), which would be tailored to transversely isotropic materials to numerically calculate E_{33} and G_{13}, through curve fitting (Kelleher et al., 2012). This analysis will be the subject

of future work. The main limitation of the presented anisotropy index is that it is calculated based on isotropic models of indentation. However, this index can be used to compare the anisotropy in different VF samples, especially in small tissue engineering constructs where information about the anisotropic properties of the VF tissue is desirable to assess the effective remodeling during wound healing or tissue engineering.

Spatial variations of the mechanical properties have a significant effect on the physiology of the VF tissue, the anisotropic properties, and in turn the VF vibration characteristics. Local mechanical properties are needed to study VF mechanobiology and predict the outcome of voice training for the treatment of voice disorders (Li et al., in press). A comparison between porcine (Fig. 2 and Miri et al., 2013), and human NLSM results (Miri et al., 2012c) suggests that porcine VFs are much less differentiated than human VFs. The special homogeneity of VF tissue along anterior–posterior direction was subject of pervious research (Dollinger et al., 2011; Kelleher et al., 2010). Similar to our results, point force excitations (Dollinger et al., 2011) showed that stiffness increases from the central region to the cartilaginous anterior–posterior ends for human tissue, in contrast with those of tensile test (Kelleher et al., 2010). Finite element models have shown that anisotropy affects the eigenfrequencies of VF tissue (Kelleher et al., 2010). The accurate characterization of the anisotropic properties of VF tissue is needed for the design of implants and artificial organs.

4.3. *Permeability of VF tissue*

Diffusivity and permeability coefficients were calculated using Eqs. (12), (14) and (15). Small differences were found between the diffusivity coefficients in different layers. An isotropic poroelastic model was used. Hydraulic permeability originates from the interaction of tissue structure and fluid movement. Fluid is inherently isotropic. The solid part is composed of negatively charged glycosaminoglycans (e.g., hyaluronic acid), biglycan, and fibrillar proteins (e.g., collagen and elastin). Water flow is dominated by negatively charged nonfibrilar matrix molecules, which are usually distributed isotropically in the tissue. Therefore, isotropic poroelastic models yield a good approximation of tissue behavior.

The protocol presented in this paper has several advantages. The tests are performed under water, which minimizes possible artifacts from dehydration. Freezing the samples before cutting results in very low surface roughness, on the order of 10–200 nm, contributing to higher accuracy. Nonlinear microscopy of the samples provided sufficient data to select the optimum probe size capable of capturing matrix-wide mechanical properties. The force resolution of the AFM permitted the use of smaller probes for viscoelastic characterization of the matrix. No chemical treatment was done on the tissue prior to the indentation tests.

This protocol can simply be applied to human VFs to elucidate some very important physiological phenomena in voice production. Dehydration of human VFs during phonation or smoking critically depends on the diffusion of water across different VF layers. The application of this protocol may shed light on the underlying dehydration mechanisms. Another important application of poroelastic measurements is the development of injectable drugs and gels used for treating VF disease. A knowledge of diffusion properties can help predict drug and biomaterial diffusion in treated VFs.

5. Conclusion

An experimental procedure was developed to measure the anisotropic mechanical properties and the diffusivity coefficient of the VF tissue through AFM-based indentation and creep tests. Porcine VF tissue was dissected, snap-frozen and cut in different layers and orientations. The tissue was found to be more compliant near the center, away from the cartilaginous ends. Anisotropic indentation along two perpendicular planes yielded an anisotropy index of AI=2.47. Assuming a transversely isotropic material, indentation gives elastic constants of $E_{22}=E_{11}=1.7\pm1$ kPa along the transverse directions. This protocol may have significant applications for the local mechanical characterization of human VFs and tissue engineered constructs, the characterization of small-scale tissue (e.g., rat VFs), and the design of biomaterials and drugs with known diffusivity and mechanical properties for VF treatment.

Acknowledgments

This work was financially supported by National Institute of Health Grant R01-DC005788 (Luc Mongeau, principal investigator). The authors thank Professor Paul W. Wiseman (Physics Department, McGill University, Montreal) for sharing his NLSM system.

REFERENCES

Alipour, F., Jaiswal, S., Vigmostad, S., 2011. Vocal fold elasticity in the pig, sheep, and cow larynges. Journal of Voice 25, 130–136.

Athanasiou, K.A., Zhu, C.F., Wang, X., Agrawal, C.M., 2000. Effects of aging and dietary restriction on the structural integrity of rat articular cartilage. Annals of Biomedical Engineering 28, 143–149.

Bakhshaee, H., Young, J., Yang, J.C.W., Mongeau, L., Miri, A.K., 2013. Determination of strain field on the superior surface of excised larynx vocal folds using DIC. Journal of Voice, http://dx.doi.org/10.1016/j.jvoice.2013.05.009.

Butt, H.J., Cappella, B., Kappl, M., 2005. Force measurements with the atomic force microscope: technique, interpretation and applications. Surface Science Reports 59, 1–152.

Chhetri, D.K., Zhang, Z., Neubauer, J., 2011. Measurement of Young's modulus of vocal folds by indentation. Journal of Voice 25, 1–7.

Dollinger, M., Berry, D.A., Huttner, B., Bohr, C., 2011. Assessment of local vocal fold deformation characteristics in an in vitro static tensile test. Journal of the Acoustical Society of America 130, 977–985.

Ebenstein, D.M., Pruitt, L.A., 2006. Nanoindentation of biological materials. Nano Today 1, 26–33.

Fan, Z., Swadener, J.G., Rho, J.Y., Roy, M.E., Pharr, G.M., 2002. Anisotropic properties of human tibial cortical bone as measured by nanoindentation. Journal of Orthopaedic Research 20, 806–810.

Galli, M., Oyen, M.L., 2009. Fast identification of poroelastic parameters from indentation tests. Computer Modeling in Engineering and Sciences 48, 241–270.

Hahn, M.S., Kobler, J.B., Zeitels, S.M., Langer, R., 2006a. Quantitative and comparative studies of the vocal fold extracellular matrix I: elastic fibers and hyaluronic acid. Annals of Otology, Rhinology, and Laryngology 115, 156–164.

Hahn, M.S., Kobler, J.B., Zeitels, S.M., Langer, R., 2006b. Quantitative and comparative studies of the vocal fold extracellular matrix II: collagen. Annals of Otology, Rhinology, and Laryngology 115, 225–232.

Heris, H.K., Rahmat, M., Mongeau, L., 2012. Characterization of a hierarchical network of hyaluronic acid/gelatin composite for use as a smart injectable biomaterial. Macromolecular Bioscience 12, 202–210.

Itskov, M., Aksel, N., 2002. Elastic constants and their admissible values for incompressible and slightly compressible anisotropic materials. Acta Mechanica 157, 81–96.

Johnson, K.L., 1987. Contact Mechanics. Cambridge University Press.

Kaster, T., Sack, I., Samani, A., 2011. Measurement of the hyperelastic properties of ex vivo brain tissue slices. Journal of Biomechanics 44, 1158–1163.

Kelleher, J.E., Siegmund, T., Du, M., Naseri, E., Chan, R.W., 2012. Empirical measurements of biomechanical anisotropy of the human vocal fold lamina propria. Biomechanics and Modeling in Mechanobiology, 1–13.

Kelleher, J.E., Zhang, K., Siegmund, T., Chan, R.W., 2010. Spatially varying properties of the vocal ligament contribute to its eigenfrequency response. Journal of the Mechanical Behavior of Biomedical Materials 3, 600–609.

Li, N.Y.K., Heris, K., Mongeau, L., H., 2013. Current understanding and future directions for vocal fold mechanobiology. Journal of Cytology and Molecular Biology, 1.

Lin, D.C., Dimitriadis, E.K., Horkay, F., 2007. Robust strategies for automated AFM force curve analysis: I. Non-adhesive indentation of soft, inhomogeneous materials. Journal of Biomechanical Engineering 129, 430–440.

Lin, D.C., Shreiber, D.I., Dimitriadis, E.K., Horkay, F., 2009. Spherical indentation of soft matter beyond the Hertzian regime: numerical and experimental validation of hyperelastic models. Biomechanics and Modeling in Mechanobiology 8, 345–358.

Loparic, M., Wirz, D., Daniels, A.U., Raiteri, R., Vanlandingham, M.R., Guex, G., Martin, I., Aebi, U., Stolz, M., 2010. Micro- and nanomechanical analysis of articular cartilage by indentation-type atomic force microscopy: validation with a gel-microfiber composite. Biophysical Journal 98, 2731–2740.

Miri, A.K., Barthelat, F., Mongeau, L., 2012a. Effects of dehydration on the viscoelastic properties of vocal folds in large deformations. Journal of Voice 26, 688–697.

Miri, A.K., Heris, H.K., Tripathy, U., Wiseman, P.W., Mongeau, L., 2013. Microstructural characterization of vocal folds toward a strain–energy model of collagen remodeling. Acta Biomaterialia http://dxdoi.org/10.1016/j.actbio.2013.1004.1044.

Miri, A.K., Mitri, F.G., 2011. Acoustic radiation force on a spherical contrast agent shell near a vessel porous wall: theory. Ultrasound in Medicine and Biology 37, 301–311.

Miri, A.K., Mongrain, R., Chen, L.X., Mongeau, L., 2012b. Quantitative assessment of the anisotropy of vocal fold tissue using shear rheometry and traction testing. Journal of Biomechanics 45, 2943–2946.

Miri, A.K., Tripathy, U., Mongeau, L., Wiseman, P.W., 2012c. Nonlinear laser scanning microscopy of human vocal folds. The Laryngoscope 122, 356–363.

Nia, H.T., Han, L., Li, Y., Ortiz, C., Grodzinsky, A., 2011. Poroelasticity of cartilage at the nanoscale. Biophysical Journal 101, 2304–2313.

Oliver, W.C., Pharr, G.M., 1992. Improved technique for determining hardness and elastic modulus using load and displacement sensing indentation experiments. Journal of Materials Research 7, 1564–1580.

Oliver, W.C., Pharr, G.M., 2004. Measurement of hardness and elastic modulus by instrumented indentation: advances in understanding and refinements to methodology. Journal of Materials Research 19, 3–20.

Rahmat, M., Hubert, P., 2010. Interaction stress measurement using atomic force microscopy: a stepwise discretization method. Journal of Physical Chemistry C 114, 15029–15035.

Reisinger, A.G., Pahr, D.H., Zysset, P.K., 2011. Principal stiffness orientation and degree of anisotropy of human osteons based on nanoindentation in three distinct planes. Journal of the Mechanical Behavior of Biomedical Materials 4, 2113–2127.

Stolz, M., Raiteri, R., Daniels, A.U., VanLandingham, M.R., Baschong, W., Aebi, U., 2004. Dynamic elastic modulus of porcine articular cartilage determined at two different levels of tissue organization by indentation-type atomic force microscopy. Biophysical Journal 86, 3269–3283.

Swadener, J.G., Pharr, G.M., 2001. Indentation of elastically anisotropic half-spaces by cones and parabolae of revolution. Philosophical Magazine A: Physics of Condensed Matter, Structure, Defects and Mechanical Properties 81, 447–466.

Swadener, J.G., Rho, J.Y., Pharr, G.M., 2001. Effect of anisotropy on elastic moduli measured by nanoindentation in human tibial cortical bone. Journal of Biomedical Materials Research 57, 108–112.

Tao, C., Jiang, J.J., Zhang, Y., 2009. A fluid-saturated poroelastic model of the vocal folds with hydrated tissue. Journal of Biomechanics 42, 774–780.

Titze, I.R., Talkin, D.T., 1979. A theoretical study of the effects of various laryngeal configurations on the acoustics of phonation. Journal of the Acoustical Society of America 66, 60.

Wallis, L., Jackson-Menaldi, C., Holland, W., Giraldo, A., 2004. Vocal fold nodule vs. vocal fold polyp: answer from surgical pathologist and voice pathologist point of view. Journal of Voice 18, 125–129.

Weiß, S., Thomson, S., Lerch, R., Döllinger, M., Sutor, A., 2012. Pipette aspiration applied to the characterization of nonhomogeneous, transversely isotropic materials used for vocal fold modeling. Journal of the Mechanical Behavior of Biomedical Materials.